RoboScallop: A Bivalve Inspired Swimming Robot

Matthew A. Robertson, Filip Efremov, and Jamie Paik

***Abstract*—Underwater swimming robots permit remote access to over 70% of the Earth's surface that is covered in water for a variety of scientific, environmental, tactical, or industrial purposes. Many practical applications for robots in this setting include sensing, monitoring, exploration, reconnaissance, or inspection tasks. In the interest of expanding this activity and opportunity within aquatic environments, this letter describes the development of a swimming robot characterized by simple, robust, and scalable design. The robot, named RoboScallop, is inspired by the locomotion of bivalve scallops, utilizing two articulating rigid shell components and a soft elastic membrane to produce water jet propulsion. A single-DoF, reciprocating crank mechanism enclosed within the shell housing of the robot is used to generate pulsating thrust, and the performance of this novel swimming method is evaluated by characterization of the robot jet force and swimming speed. This is the first time jet propulsion is demonstrated for a robot swimming in normal, Newtonian fluid using a bivalve morphology. We found the metrics of the robot to be comparable to its biological counterpart, but free from metabolic limitations which prevent sustained free swimming in living species. Leveraging this locomotion principle may provide unique benefits over other existing underwater propulsion techniques, including robustness, scalability, resistance to entanglement, and possible implicit water treatment capabilities, to drive the further development of a new class of self-contained, hybrid-stiffness underwater robots.**

***Index Terms*—Biologically-inspired robots, marine robotics, soft robot materials and design.**

I. Introduction

UNDERWATER robots, classified as either autonomous underwater vehicles (AUVs) or remotely operated vehicles (ROVs), have been used for exploration, reconnaissance, or sensing and monitoring [1]–[8] of remote areas which are otherwise difficult to access. In the wake of disasters, these robots have been deployed for search and rescue efforts to locate and survey wreckage sites, or to evaluate and mitigate potential future risks from water contamination or other hazards such as mines [9]. In other scenarios, robots have provided means to identify and study lost or sunken archaeological artifacts [10], and for unobtrusive scientific observation of animal behavior [11]. More frequently, underwater robots are being deployed for inspection tasks to evaluate condition of critical infrastructure. With water environments comprising over 70% of the Earths surface, and the economic value of aquatic activity in oceans and lakes for the US alone estimated at $352 billion in gross domestic product (2% of total GDP) for 2014 [12], the clear importance of proficiency in marine logistics underscores the demand for capable robots and technology suited to this domain.

In the broadest terms, underwater robots can be categorized into two main types by the strategy they utilize for locomotion: propeller driven and bioinspired swimmers. The former category includes the widest selection of underwater robots (and other water vehicles in general) by far, for which their basic drive method the use of motorized spinning propellers - can be seen as the standard method for underwater locomotion and navigation [13]. In contrast to this conventional approach, the latter category includes a more diverse set of robots which utilize alternative mechanisms to derive propulsion under water. These actions can be described holistically as swimming, not only to differentiate from the other primary underwater locomotion method, but in part because they more closely resemble the natural actions and propulsion methods of biological animals described in the same way.

The majority of swimming robots are inspired by fish locomotion, with a variety of different swimming methods corresponding to an equivalent variety of species [14]. Some robots utilize the method of anguilliform swimming, generating low pressure zones along the body for thrust using whole-body wave motions, similar to lamprey and eels [15]–[17]. Other robots employ the more familiar carangiform method of body-coupled, tail driven swimming patterns to provide thrust analogous to the style of salmon, trout, or tuna [18], [19]. Completing the spectrum of fish inspired swimming techniques, another set of robots have leveraged the ostraciiform method which only directly uses the tail fin to generate thrust, as with the boxfish [20], [21].

An alternative bioinspired swimming method gaining interest for use in underwater robots is jet propulsion. This method has been explored through the development of synthetic jets [22]–[27] to power underwater systems, as well as others which leverage biologically inspired morphology, including soft bodied robots inspired by cephalopods [28]–[30]. This form of thrust generation has attracted attention for its relative simplicity, robustness, and low-speed control fidelity in comparison to other methods [31]. A particular benefit of these qualities make jet propulsion an ideal candidate for producing small-scale robotic systems, either for use in constrained environments or in swarm applications which draw advantages from redundancy and large area coverage in low-cost, distributed robotic networks [32]–[34].

A small variety of simple, small-scale, and low-cost robots have drawn inspiration from lesser known jet-propelled

Manuscript received September 10, 2018; accepted December 28, 2018. Date of publication February 4, 2019; date of current version March 5, 2019. This work was supported in part by the Swiss National Science Foundation (SNSF) and in part by the National Centre of Competence in Research (NCCR) Robotics (Switzerland). This letter was recommended for publication by Associate Editor B. Mazzolai and Editor Y. Sun upon evaluation of the reviewers' comments. *(Corresponding author: Jamie Paik.)*

The authors are with the Reconfigurable Robotics Laboratory, Institute of Mechanical Engineering, School of Engineering, Ecole Polytechnique Federale de Lausanne, Lausanne CH-1015, Switzerland (e-mail: matthew.robertson@epfl.ch; efremov.filip.fe@gmail.com; jamie.paik@epfl.ch).

This letter has supplementary downloadable material available at http://ieeexplore.ieee.org provided by the authors. The Supplemental Materials contain a video showing two versions of the RoboScallop prototype swimming underwater. This material is 3.76 MB in size.

Digital Object Identifier 10.1109/LRA.2019.2897144

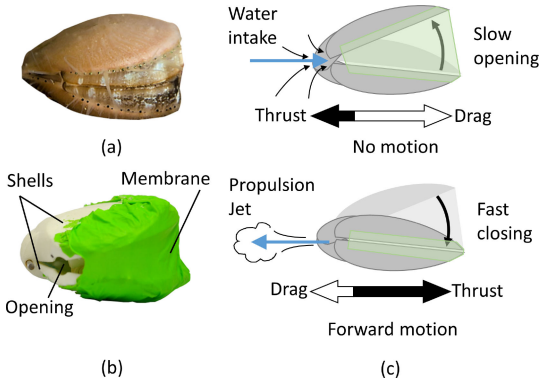

Fig. 1. Scallop inspired robot locomotion. The morphology and function of a biological scallop depicted in (a) are reflected in the robot prototype shown in (b) which consists of two shells connected at a hinge and enclosed by a flexible elastic membrane. The robot and animal both achieve swimming by rapid, cyclic opening and closing of their shells to generate water jet thrust for propulsion. When the robot shells open, water is drawn into the body interior through rear openings near the hinge. Upon more rapid shell closing, the water is forced out backwards to produce a reaction force which facilitates net forward motion (c).

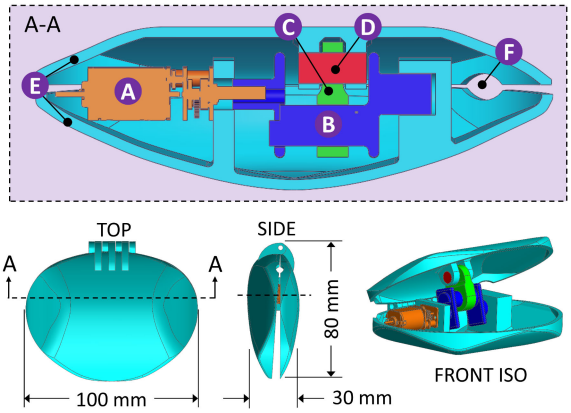

Fig. 2. Mechanical overview of RoboScallop prototype. A 3D CAD model of the robot is shown in different views with a cross section through A-A depicting the critical components of the internal mechanism of the robot: A-motor, B-crankshaft, C-connecting arm, D-hinge pin, E-body shells, and F-intake/jet aperture. The front covering membrane is not shown.

swimmers of the underwater animal world, belonging to the class of bivalve mollusks. Scallop-inspired microscopic swimming robots exploit the dynamics of non-Newtonian liquids to generate forward motion from an induced change in fluid viscosity surrounding the robot [35]. While taking cues from their biological counterpart for overall shape and cyclic flapping or "clapping" motion behavior, these robots do not directly employ the fluid dynamic principles which drive natural scallop swimming. In nature, this capability is achieved by producing jets which propel the scallop forward via momentum exchange with high velocity water through two holes near the hinge of its upper and lower shells. While opening its shells, the scallop intakes water through soft, extensible velar lobes which are separated across the top and bottom of the large front opening. To perform a swimming stroke, the scallop rapidly closes from its fully opened position. During this rapid closing, the flexible lobes make contact across the shells sealing water in, causing the pressure inside the scallop to rise and propulsive jets to form out of the smaller openings near the rear hinge [36]–[40].

No robots are known to explicitly leverage the morphology and swimming technique of scallops as found in nature, however this method would enable systems which are a unique combination of robust to hazards or sustained use, safe in delicate environments, and simple by design. Scallop-inspired robots offer useful potential as an alternative to existing underwater robots which either pose risks of entanglement, environmental damage, or disruption, or feature more complex design and functional structure. Emulating natural animal behavior and comprising minimal moving parts, this robot concept illustrated in Fig. 1 may find use in standard underwater AUV applications, including remote sensing, monitoring, and exploration, or in a variety of specialized tasks conducting work in delicate ecosystems or use in underwater robot swarms.

A. Objectives

In this work, a bioinspired robot, RoboScallop, is described which leverages the swimming principle employed by bivalve organisms for underwater locomotion. A simple, single-DoF mechanism for generating cyclic opening and closing of the structural valve, or shell, components of the robot is employed, while the use of a thin, stretchable membrane enables asymmetric impulse generation from water jet thrust for net forward motion. To quantify the utility of the robot for practical underwater robotic applications, its performance is characterized by measuring the jet force produced and the resultant swimming speed. Various benefits of the robot locomotion mechanism and morphology are discussed, including amenability to manufacturability and scalability through the use of a wide variety of methods and materials and various alternative drive mechanisms or low-cost robot swarms, hermetically sealed design, robustness in cluttered environments, and potential suitability for functional applications to actively filter or treat polluted water environments. In summary, we will demonstrate (1) a robust underwater swimming robot design based on the morphology and functionality of bivalve animals, including scallops, (2) forward thrust generated by a simple, single-DoF crank mechanism, and configuration dependent asymmetric drag, and (3) validation of locomotion effectiveness by experimental measurement of prototype robot in free swimming speed up to 16 cm/s (2 BL/s) with measured propulsion thrust of 1 N.

II. Mechanical Design

The RoboScallop robot approximates the morphology of a biological swimming scallop bivalve mollusk, consisting of two articulated shells, a soft, water-sealed connecting membrane structure spread between them, and single motor actuator as seen in Fig. 2. Swimming is achieved via cyclic opening and closing (flapping) of the shells which draws water into the enclosed volume of the robot interior on the intake stroke (opening) and subsequently forces water out of openings at the rear to produce thrust. While the robot prototype is operated underwater, it receives electrical power through a tether of thin, insulated wire from a power supply located outside the water. Weight was minimized where possible in the design to enable faster swimming speeds, however the mass of all components was not distributed symmetrically across the robot. To offset the weight and balance its distribution, small pieces of closed cell insulation foam were glued to the inside of the shell strategically, until stable, neutral buoyancy was achieved.

TABLE I
ROBOSCALLOP PROTOTYPE PARAMETERS

PROPERTY	SPECIFICATION
Dimensions	$80 \times 100 \times 30$ mm
Mass	65 g
Speed	16 cm/s or 2 BL/s (max)
Clapping frequency	2.6 Hz (max)
Actuators	Pololu HPCB Micro Metal Gearmotor, 100:1
Power	12 V, 380 mA (typical), 560 mA (peak)

A. Body Components

Two rigid shells define the outer body shape of the robot, and provide structure for mounting the mechanical components used to generate cyclic opening and closing, or flapping motion used in swimming. The shell components and integrated interior mounting structures were manufactured by fused-filament 3D printing of ABS plastic. A shell thickness of 2 mm was utilized to ensure sufficient rigidity under loading from the interior crank mechanism without causing visible deformation of the shell, while also maintaining low mass to achieve greater swimming performance. This dimension was chosen experimentally through various prototype iterations however, and was not formally optimized to maximize strength or minimize weight. The physical parameters of the robot are summarized in Table I.

The overall contour and size of the body was modeled after the shape of scallop shells to reduce drag in water and achieve hydrodynamic efficiency at least similar to that of biological counterparts. A flow simulation using a 3D model of the shell and Solidworks Flow Simulation software was conducted to assess the drag coefficient of the designed body shape at different opening positions in constant fluid flow. The results of the simulation analysis are shown in Fig. 3(a) and indicate roughly linearly increasing drag for increasing shell opening angles. While the forward motion of scallops can be directly attributed to the thrust produced by water jets for propulsion, the difference in drag at different opening angles in relation to varying points of the swim cycle also indirectly contributes to enhance this net forward progress. When the robot shells are open, drag is at a maximum and forward thrust is at its minimum. When the shells are closed following a power stroke, forward thrust is approximately at its maximum. In this way, with complementary, inverted cycles of drag and thrust, resistance to forward motion is minimized. At the same time, the increased drag at different shell angles is expected to oppose motion in the reverse direction with the opposite trend. During the shell opening phase of the swimming cycle, the reverse thrust is at maximum when the drag is also maximum, and similarly minimal when the drag is also minimal. These phases are illustrated in Fig. 3(b). This convenient characteristic of drag beneficially coupled to thrust cycles plays a unique role in facilitating unidirectional forward swimming in scallop inspired locomotion.

A continuous, elastic membrane made from 0.1 mm thick synthetic soft nitrile polymer spans the opening of the articulated shells to seal the inner volume of the robot along the front edge where it is affixed in place with cyanoacrylate glue. The function of the membrane is similar to that of the velar lobes of biological scallops, with the exception that it is always intact and covering the front opening of the robot. With the membrane affixed in this way in contrast to the natural configuration of scallops, water enters the shells from the the rear of the robot rather than the front. When the shells start to close, all of the internal water is pressurized against the shell sides of the robot as well as the membrane. The membrane limits water from escaping through the front and forces it back inside the robot and out through rear aperture holes 4 mm in height and 10 mm in width to the sides of the hinge connecting both shells.

In addition to directing the flow of water used for thrust, the membrane helps to also balance moments produced by external hydrodynamic forces which develop over the shells during swimming. These forces have been studied and modeled in previous work for biological scallops with comparable morphology to the robot prototype [41]. As described for scallops, a velocity dependent effect termed pseudo-viscosity acts to continually open the shells of the robot when moving forward. The force of the membrane as it stretches during opening resists this moment, reducing the shell opening speed and torque load on the motor during closing. Additionally, external hydrodynamics produce an asymmetric pseudo-elasticity torque effect proportional to shell angle, which assists in opening but resists shell closing. Again, the membrane acts to balance the moment from these external forces, resisting the opening force and assisting in closing to increase the closing speed and reduce the speed of opening.

For the RoboScallop prototype robot, the difference in the duration of these events, with slower shell opening times and faster closing, helps produce greater thrust from water expulsion on the closing stroke than that from low pressure at the rear shell apertures generated on opening. Although this difference is not the main mechanism attributed to biological scallop swimming, it becomes a dominant factor for the robot which cannot intake water from the front.

B. Reciprocating Mechanism

The opening and closing of the robot is enabled by a 3D printed crank mechanism which is powered by a 12 V DC motor. The motor was chosen primarily because of its weight (9.5 g), size ($10 \times 12 \times 26$ mm), and speed (330 rpm, free) which roughly corresponds at 5.5 Hz to the frequency of biological scallop swimming of 3-5 H [21]. No effort was made to isolate or seal the motor and its internal components from water penetration, which allowed only short term use of the gearmotor before replacement was necessary. The mechanical structure of the prototype including the crank mechanism and body shells are shown in Fig. 2.

III. PRINCIPLES OF ROBOSCALLOP LOCOMOTION

The equation for thrust, T, can be borrowed from previous literature on squid locomotion to describe the mechanism of swimming for the RoboScallop [42], as shown in Eq. 1. Both species produce thrust from momentum exchange with water ejected at their rear through small openings, derived from a single pressurized cavity contained within the animal body which is filled and expelled cyclically.

$$T = \rho Q u = \frac{\rho Q^2}{A} = \frac{\rho}{A}\left(\frac{\Delta V}{\Delta t}\right)^2 \tag{1}$$

In this equation, Q and u are the flow rate and velocity of the water through the jet orifice, respectively, and ρ is the water density. The volumetric flow rate can be represented by $Q = \Delta V/\Delta t$ as the change in cavity volume, V, over a corresponding change in time t, and the velocity can be written as

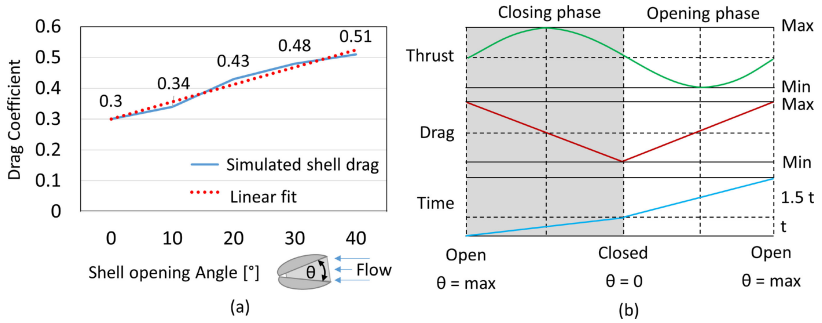

Fig. 3. Steady state flow simulation of shell drag. Larger opening angles correspond to larger predicted drag coefficients (a). Drag is only considered from flow induced by relative motion of the robot in the forward direction (inset figure, indicated by arrows), which contributes to the net force acting on the robot during swimming; drag decreases during forward jet thrust (closing phase) and increases only during water intake while the shells are opening, as qualitatively illustrated in (b). A representative plot of the average opening and closing times for a single period of the swimming cycle is shown with a ratio of approximately 1.5:1.

$u = Q/A$. The variable A represents the cross sectional area of the jet orifice.

Like squid, since a single orifice at the rear of the RoboScallop is used for both water intake and jet propulsion, thrust is produced in both strokes of a swimming cycle but in opposite directions. The main condition for achieving net forward motion is that the forward thrust from jet propulsion during shell closing is greater than that from intake during shell opening, or $T_{closing} > T_{opening}$. Due to the cyclic swimming motion, $\Delta V_{closing} = \Delta V_{opening}$ and Eq. (1) simplifies to

$$\Delta t^2_{opening} A_{opening} > \Delta t^2_{closing} A_{closing} \tag{2}$$

which indicates that the magnitude of thrust produced is primarily a function of the time duration of the water jet, and the area of the orifice through which the jet is formed. If the area of the orifice is equal or nearly similar for both the opening and closing stroke, the net thrust is dictated by the difference in time spent during each phase, where faster relative closing time results in forward jet propulsion. Alternatively, equal phase timing can still produce net forward thrust over a swimming cycle by modulating the size of the orifice, reducing the cross sectional area during the closing stroke and increasing it during the opening, refill stroke.

Due to the fixed size of the shell orifice and the symmetry imposed by the cyclic mechanism for driving the shells, the RoboScallop employs only the first of these strategies to generate forward thrust. A difference in timing is, however, observed between opening and closing, and is indeed designed into the device through two main features: the orientation of the inner crank mechanism which produces asymmetric, non-harmonic oscillation as well as the presence of the elastic membrane across the shells which acts to resist motion in opening and assist in closing. From video tracking analysis, the ratio of opening times to closing times was found to be approximately 1.5:1, where the time interval of each phase was averaged from multiple successive video frames.

Scallops, in comparison, generate most of their thrust only in the forward direction by expelling water through rear jets, and by taking water in from the sides and front. We define the scallop swimming cycle as having only these two distinct phases, distinguished by the relative direction of shell motion either toward (closing) or away (opening) from each other. The effect of timing in the opening and closing phases of scallop swimming is not regarded as the dominant contribution to forward thrust, although it has been attributed to some portion of it. A difference in timing is observed in natural scallop swimming when these two phases are defined strictly by shell angular velocity [38]. Further evidence of this differential phase timing effect also exists in [39], where increases in whole-body performance metrics were measured (faster swimming speeds and higher acceleration) in association with decreased closing (adduction) times relative to opening (abduction) at higher environmental temperatures. Even for non-jetting species such as jellyfish, differential timing in cyclic swimming is also leveraged for locomotion, and has been demonstrated through prototypes in prior work [43], [44].

IV. Experiments

A. General Testing Procedure

For all tests, electrical power was provided through a two-wire tether (1 m) from a power supply, routed symmetrically through the back side of the robot with one wire on each side of the hinge. To avoid physical interference with the robot during testing, the main power switch of the power supply was used for control, to activate and deactivate the drive motor. For the long distance free swimming test, an extra long tether (3 m) of flexible wire was utilized for extended range of motion.

For each of the three main tests conducted at different times and described in following sections, a new DC gearmotor was used to reduce the effect of component degredation on robot performance. While this may have introduced other effects from variability in the specific motor components and general robot assembly affecting any differences between tests, this is expected to be less than the effect from motor corrosion, which led to observable loss of speed and power between consecutive days of use.

B. Blocked Force Jet Characterization

The force created by the propulsive jets was measured by placing the robot in a rigid harness suspended from above into a benchtop water tank to simulate a blocked force swimming condition. The top of the harness was attached to a Nano17, 6-axis load cell mounted above and outside of the water, which measured the force output of the robot produced by cyclic shell flapping. The harness and the robot were connected underwater through the shell hinge joint to prevent rotation of the robot along its horizontal and vertical axis. Rotation of the robot body about the axis of the hinge joint was limited by a bar supporting it in a horizontal resting position. The shells of the robot were still free

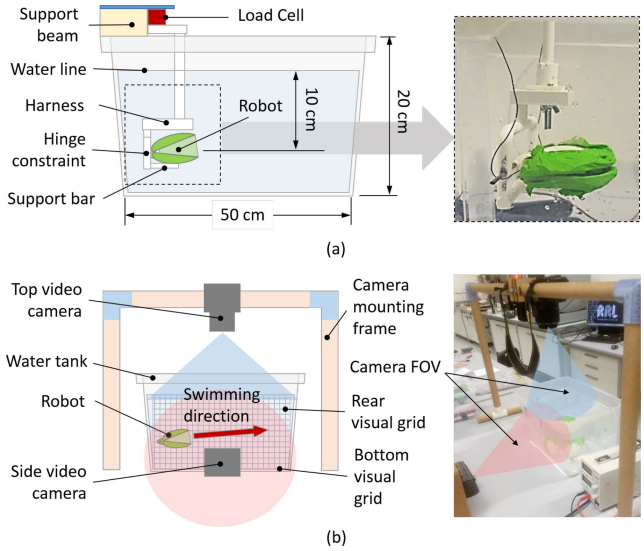

Fig. 4. Experimental setups. The jet thrust blocked force test setup is depicted in (a). The test was conducted in a benchtop water tank using a rigid 3D printed harness to connect the robot held under water to a load cell mounted outside of the water. The free swimming speed test setup is shown in (b). Video cameras positioned above and in front of the translucent water tank captured the swimming trajectory of the robot for a series of swimming trials. The speed of the robot was estimated using video time data and a background grid pattern behind and below the tank, visible within each camera's field of view (FOV) for distance calibration.

to open and close as in normal swimming conditions since the motion of the upper shell was not impinged. The experimental setup can be seen in Fig. 4(a).

Measurements of the propulsive force were taken at different flapping frequencies, which were set by supplying a range of DC voltages to the mechanism drive motor. Within the operating range of the motor from 6 V to 12 V, measurements were taken at 2 V increments for a total of four trials. This voltage range corresponded to flapping frequencies ranging from 1.4 to 2.6 Hz. For each trial, the robot was run in the test setup described above for at least 10 cycles of flapping while the force on the load cell was logged continuously at a rate of 100 Hz, more than an order of magnitude above the expected flapping frequency.

The blocked force load cell measurements for each different flapping frequency trial were first segmented into single strokes identified by peaks in the qualitatively sinusoidal data. The ten individual strokes per trial were then interpolated and averaged to obtain a representative force profile over time for every condition. This profile was then analyzed by taking its time integral to calculate the impulse per stroke (one period), and by measuring the time T of the average profile to calculate the measured flapping frequency f as $1/T$. A separate integral was taken over the positive and negative force regions of each profile to yield positive, J_{pos}, and negative, J_{neg}, impulse produced, respectively. These values were summed to also obtain a net impulse, J_{net}, which determines the ultimate trajectory of the robot, with positive net impulse values corresponding to forward motion.

C. Swimming Speed Characterization

The speed of RoboScallop in free swimming was measured at different operating voltages, corresponding to different clapping frequencies, as described in the jet force characterization section. The benchtop water tank was again used but the robot was not constrained by a harness. The experimental setup is shown in Fig. 4(b). For the highest clapping frequency and resulting jet force, at least 10 swimming cycles were possible across the length of the tank. Measurements of the robot position were taken using video cameras and a visible background grid pattern comprised of one centimeter spaced lines for scaling reference. The grid was used to measure the distance traveled by the robot, marked by the joint center of the shell hinge, over a duration of elapsed time obtained from the difference between frame timestamps of the recorded video. The straight line distance between initial and final positions from the side view was used to calculate the speed over the measured timeframe, and accounted for motion in the horizontal and vertical plane. Lateral position deviations were neglected in this measurement of speed as the majority of motion produced by the jet propulsion was observed to be in the forward and upward directions. This test was repeated at least 5 times for each voltage input and from these quantities an average speed measurement was determined.

A second, simplified robot prototype was also tested to demonstrate to an extent the effect of outer shell shape on swimming speed. While all other aspects of its mechanical design remained equivalent to the biologically inspired design, this prototype featured square edged shells and a box-like shape. Three swimming trials were conducted in the benchtop water tank, and visually recorded with a camera in the same setup used in prior experiments.

D. Free Swimming

A large (2 m $\times$ 6 m), shallow (30 cm depth) indoor pool was used to allow the robot to swim greater distances than possible in the benchtop water tank. This test was performed to visualize and study the performance of the robot in a more realistic setting of a large body of water, to minimize possible effects from water jet and flow interference with the tank walls. A waterproof GoPro Hero3 camera with a wide angle lens was used to capture the swimming behavior of the robot from underwater, set back the full width of the pool away to obtain the longest possible continuous recording as the robot swam across the camera in the direction of the pool length. No grid pattern or calibration features were used in this test to calculate speed, but overall distance traveled and average speed was estimated using the body length as a scale. The accuracy of this method was limited however, since the robot was observed to turn as it swam and the motion was not captured by the underwater camera which was alongside the robot, in the plane of the lateral deviation.

V. Results

A. Jet Force

Our robot was shown to generate asymmetric thrust, with greater forward impulse than in the reverse direction, to achieve net forward motion. The quantified results of the jet force characterization test are shown in Fig. 5. The robot produced a maximum peak thrust of 1.00 N, measured above 10 V, where the net impulse magnitude appears to saturate. In Fig. 5 b it is evident that above this control voltage corresponding to a swimming frequency of 1.4 Hz, the value of net impulse remains generally constant. The thrust measured closely matches results from similar experiments with biological scallops which generated 1.15 N of thrust impulse [39].

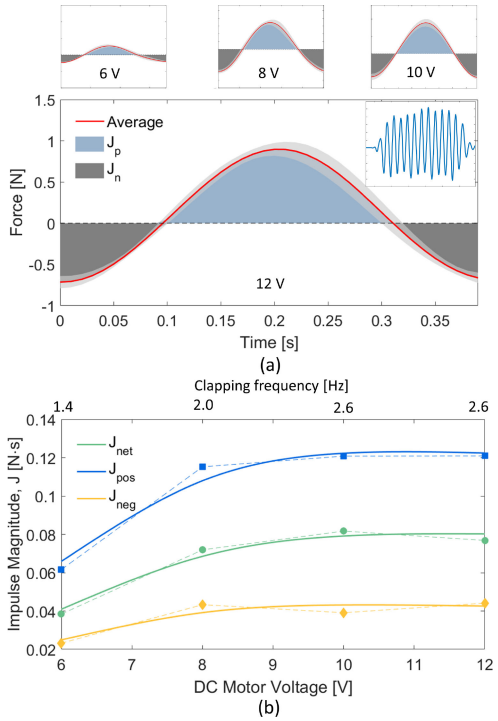

Fig. 5. Jet force profile and thrust impulse in blocked force test. The average force output of the RoboScallop prototype over a 10 cycle blocked force test is shown in (a) with shaded regions representing the impulse produced. The test was repeated for several operating voltages between 6 and 12 V, yielding different flapping frequencies between 1.4 and 2.6 Hz. For each test, the positive and negative regions of impulse are summed to calculate a net impulse which quantifies the effectiveness of the robots locomotion. The relationship of impulse to driving frequency or DC motor voltage input is represented in (b), which indicates a limit to the thrust force produced by the robot. Square points represent the calculated impulse totals for different inputs, while the solid curve shows a spline fit.

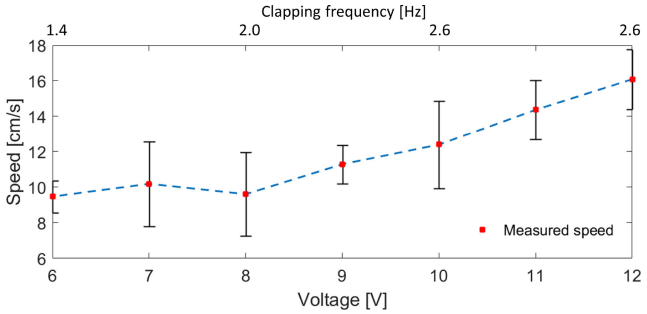

Fig. 6. Swimming speeds measured in benchtop test. The swimming speed of the biologically inspired robot prototype is shown for varying input voltages. Red points represent the average measurement while error bars depict a single standard deviation for five trials.

B. Swimming Speed

The fastest swimming speed we recorded for our robot with the benchtop water tank setup was 16 cm/s, or 2.0 Body Lengths/s (BL/s), obtained using a 12 V motor input to produce a 2.56 Hz flapping frequency. These free swimming speeds were also validated in tests conducted in a large open pool, which eliminated any effects that could have been caused by waterjet reaction force against the wall of the relatively small benchtop water tank. Fig. 6 shows the measured speeds for varying input voltages.

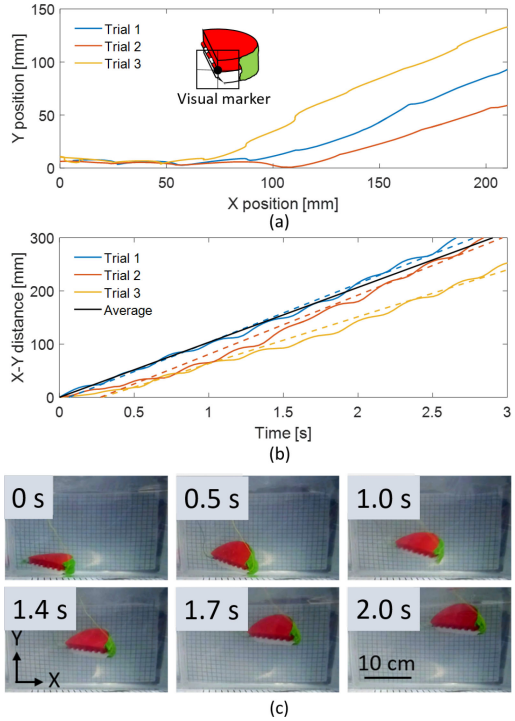

Fig. 7. Trajectory and time series of RoboScallop prototype. The displacement of a visual marker located on the robot was tracked using a video camera for three swimming trials, and is shown in (a), while this trajectory over time can be seen in (b), where the average speed was found to be 10 cm/s for the depicted trials. A time series of video frames from one trial conducted in a benchtop water tank is shown in (c) using the simplified shell shape prototype.

The simplified shell prototype also tested in the benchtop setup can be seen in Fig. 7. A linear fit was calculated for each of three swimming trials conducted, and the fits were then averaged to obtain an overall average swimming trajectory over time. The slope of this trajectory represented the average swimming speed over the three trials, and was found to be 10 cm/s or 1.3 BL/s. The results indicate a slower swimming speed with this design as expected. Notably however, vertical displacement coupled to the forward movement of the robot was also captured by the tracked marker position. While this was observed in both prototypes, the effect was most prevalent in the simplified, boxy version. In living scallops, this effect is widely known already, and used to achieve liftoff into open water from the seabed where they generally rest. Certain studies have in part attributed this directly to swimming velocity and body size [45], the former of which can be actively controlled to a degree by changing the waterjet opening at the rear of the animal, or regulated by varying the burst time of activation much like pulse width modulation. Although the exact mechanism which affects this forward and upward thrust coupling are beyond the scope of this study, it is worth future investigation as a method for underactuated control of movement in both dimensions for scallop inspired of other types of robots.

VI. Discussion

The maximum speed measured for both the biologically inspired and simplified shell design is faster than the biological *Limaria Fragilis* scallop (3.64 cm/s), and slower than *Aequipecten opercularis* (37 cm/s) [37], [39]. In part these comparisons to

biological scallops do not fully represent the performance capabilities of the robot however, as the swimming function in the animals is primarily used for short distance escape maneuvers [36], [39], and does not allow sustained swimming for long periods of time due to adductor muscle fatigue [46] combined with the relatively poor efficiency of aquatic jet-propulsion itself, cited in prior work to be a factor of roughly three times lower for squid compared to fish of similar size [38]. Although the inefficiency of locomotion is fundamental to this style of swimming and thereby an inherent limitation of this robot design, the physical limitation of muscle (or motor) saturation is not present in the robot prototype, which can operate continuously to the limit of available electrical power. The current version of the robot receives power from an off-board supply which allows indefinite use, however, it is not without the limitations of a tether. The effects of tether drag or entanglement (through water and against test barriers) were assumed negligible for characterization of swimming performance because they were performed with thin, lightweight wires in wide, smooth, and uncluttered spaces, however this feature would hinder the effectiveness of such a system in more complex environmental conditions.

Future versions for use in the real world without a tether would incorporate on-board battery power and any control electronics. While the space and power available would vary with the size of an onboard battery, the design is fundamentally adaptable to different scales. Due to the generally self-contained design without exposed moving parts, such as fins, rudders, or spinning propellers, a design which includes onboard power would also be inherently robust in cluttered environments. Scallop inspired locomotion could be beneficial where entanglement presents a risk to the robot, or in other applications where the robot might pose a risk to the environment, such as operating near and around delicate ecosystems like a coral reef. Although some simple solutions exist to improve the robustness of more conventional underwater vehicles, including the use of ducts or hubless propellers to decrease entanglement risks [47], the bioinspired RoboScallop design does not utilize high velocity spinning components and is thus less susceptible to impact from small particle debris including sand, rocks, or shells, as well as relatively more safe to any small organisms which might other be harmed by fast spinning blades.

In order to improve the practical utility of the robot prototype, future versions would also incorporate a mechanism to allow directional steering, although some applications may not require this. Biological scallops are known to exhibit directional changes during swimming that follow an alternating pattern which results in a zig-zag trajectory, thought to be useful in evading predators. This strategy was found to be voluntary and independent of clapping motion used to produce thrust [48], and thought to be the result of a mechanism in place for regulating the flow at either of the two rear hinge openings where propulsive water jets are formed, although scallops are still generally regarded as having only one primary muscle used for locomotion. In a similar way, a future robot prototype could be developed using small scale actuators (joule heated shape memory alloys) for the sole purpose of changing the area of the jet orifice to reduce or increase the exit water velocity and jet thrust produced. By changing thrust produced at each orifice independently, a mechanism for steering could be implemented without the addition of additional drive mechanisms or rudders.

A. Design Scalability and Immediate Applications

Utilizing only a reciprocating crank mechanism and a single drive motor, the simple design of the robot presented here is generally scalable to other dimensions, through various other materials, manufacturing methods, and alternative drive sources (Shape Memory Alloy actuators, voice coils, for example), although only one example robot prototype design was tested at a relatively high Reynolds number (Re). Similar to biological scallops, this prototype is relevant for swimming in fluids with Re on the order of 10^4. At very small scales, where Re is very low, the mechanism shown here may cease to function as a consequence of the Scallop Theorem that requires nonreciprocal motion as a condition for swimming in this regime. Furthermore, the efficiency of larger scallop locomotion in nature has been found to be lower than smaller ones [45]. Nevertheless, this may only be due to disproportionate scaling of mass and non-optimized hydrodynamic characteristics in animals which could be improved in engineered robots. Even without significant additions or improvements however, such robots as developed here could be used already for simple applications such as self-distributing sensor networks for communication or exploration, or water treatment operations. As the principle of operation for scallop inspired swimming is effectively that of a water pump, the integration of a filter or sensor in addition to the benefit of intrinsic mobility could offer a significant advantage in environmental cleaning or monitoring over large, remote areas utilizing a two-in-one solution. Moreover, the simplicity of the design is amenable to mass production of robot swarms to accomplish such tasks even more efficiently.

VII. Conclusion

In this letter, we studied the performance of a novel underwater locomotion method inspired by various bivalve species, including scallops, for use in expanding the accessibility and capability of operations in underwater environments. A prototype swimming robot was designed, fabricated, and tested in laboratory environments to measure the thrust generated and resulting swimming speed for different operating inputs. The experimental testing of the robot revealed the useful potential in achieving mobility with few and simple parts, suitable for developing future underwater swimming robots at various scales of size and number. These features which favor low fabrication and development costs allow such underwater robots to be employed in more locations and applications than previously feasible, leveraging the robust, bioinspired design and function adapted from bivalve swimming, compatible with a range of underwater environments.

References

[1] L. Whitcomb *et al.*, "Advances in underwater robot vehicles for deep ocean exploration: Navigation, control, and survey operations," in *Robotics Research*. London, U.K.: Springer, 2000, pp. 439–448.

[2] R. Sparrow and G. Lucas, "When robots rule the waves?," *Nav. War College Rev.*, vol. 69, no. 4, pp. 49–78, 2016.

[3] A. Crespi and A. Ijspeert, "AmphiBot II: An amphibious snake robot that crawls and swims using a central pattern generator," in *Proc. 9th Int. Conf. Climbing Walking Robots*, Jan. 2006, pp. 19–27.

[4] B. Bayat *et al.*, "Environmental monitoring using autonomous vehicles: A survey of recent searching techniques," *Current Opinion Biotechnology*, vol. 45, pp. 76–84, Jun. 2017.

[5] S. Ohata *et al.*, "Development of an autonomous underwater vehicle for observation of underwater structures," in *Proc. OCEANS MTS/IEEE*, vol. 3, Sep. 2005, pp. 1928–1933.

[6] M. K. Habib and Y. Baudoin, "Robot-assisted risky intervention, search, rescue and environmental surveillance," *Int. J. Adv. Robotic Syst.*, vol. 7, no. 1, p. 10, Mar. 2010.

[7] A. Mazumdar *et al.*, "A compact, maneuverable, underwater robot for direct inspection of nuclear power piping systems," in *Proc. IEEE Int. Conf. Robot. Autom.*, May 2012, pp. 2818–2823.

[8] E. M. H. Zahugi, M. M. Shanta, and T. V. Prasad, "Oil spill cleaning up using swarm of robots," in *Advances in Computing and Information Technology* (Advances in Intelligent Systems and Computing). Berlin, Heidelberg, Germany: Springer, 2013, pp. 215–224.

[9] C. V. Alt *et al.*, "Hunting for mines with REMUS: A high performance, affordable, free swimming underwater robot," in *Proc. MTS/IEEE Oceans. Ocean Odyssey. Conf. Proc.*, vol. 1, 2001, pp. 117–122.

[10] B. Allotta *et al.*, "The ARROWS project: Adapting and developing robotics technologies for underwater archaeology," *IFAC-PapersOnLine*, vol. 48, no. 2, pp. 194–199, Jan. 2015.

[11] N. E. Hussey *et al.*, "Aquatic animal telemetry: A panoramic window into the underwater world," *Sci.*, vol. 348, no. 6240, p. 1255642, Jun. 2015.

[12] National Oceanic and Atmospheric Administration (NOAA), "NOAA Report on the Ocean and Great Lakes Economy," NOAA Office for Coastal Management, Charleston, SC, USA, 2017. [Online]. Available: https://coast.noaa.gov/digitalcoast/training/econreport.html

[13] J. Yuh, "Design and control of autonomous underwater robots: A survey," *Auton. Robots*, vol. 8, no. 1, pp. 7–24, Jan. 2000.

[14] A. Raj and A. Thakur, "Fish-inspired robots: Design, sensing, actuation, and autonomya review of research," *Bioinspiration Biomimetics*, vol. 11, no. 3, p. 031001, 2016.

[15] C. Stefanini *et al.*, "A novel autonomous, bioinspired swimming robot developed by neuroscientists and bioengineers," *Bioinspiration Biomimetics*, vol. 7, no. 2, p. 025001, 2012.

[16] E. Kelasidi *et al.*, "Experimental investigation of efficient locomotion of underwater snake robots for lateral undulation and eel-like motion patterns," *Robot. Biomimetics*, vol. 2, no. 1, p. 8, Dec. 2015.

[17] B. Bayat, A. Crespi, and A. Ijspeert, "Envirobot: A bio-inspired environmental monitoring platform," in *Proc. IEEE/OES Auton. Underwater Vehicles*, Nov. 2016, pp. 381–386.

[18] A. D. Marchese, C. D. Onal, and D. Rus, "Towards a self-contained soft robotic fish: On-board pressure generation and embedded electropermanent magnet valves," in *Experimental Robotics* (Springer Tracts in Advanced Robotics). Heidelberg, Germany: Springer, 2013, pp. 41–54.

[19] S. F. Masoomi *et al.*, "The kinematics and dynamics of undulatory motion of a tuna-mimetic robot," *Int. J. Adv. Robotic Syst.*, vol. 12, no. 7, p. 83, Jul. 2015.

[20] P. Kodati *et al.*, "Microautonomous robotic ostraciiform (MARCO): Hydrodynamics, design, and fabrication," *IEEE Trans. Robot.*, vol. 24, no. 1, pp. 105–117, Feb. 2008.

[21] D. Lachat, A. Crespi, and A. J. Ijspeert, "BoxyBot: A swimming and crawling fish robot controlled by a central pattern generator," in *Proc. 1st IEEE/RAS-EMBS Int. Conf. Biomed. Robot. Biomechatronics*, Feb. 2006, pp. 643–648.

[22] K. Mohseni and R. Mittal, *Synthetic Jets: Fundamentals and Applications*. Boca Raton, FL, USA: CRC Press, Sep. 2014.

[23] A. P. Thomas *et al.*, "Synthetic jet propulsion for small underwater vehicles," in *Proc. IEEE Int. Conf. Robot. Autom.*, Apr. 2005, pp. 181–187.

[24] A. A. Moslemi and P. S. Krueger, "Propulsive efficiency of a biomorphic pulsed-jet underwater vehicle," *Bioinspiration Biomimetics*, vol. 5, no. 3, p. 036003, 2010.

[25] A. P. Thomas, "Exploration into the feasibility of underwater synthetic jet propulsion," Ph.D. dissertation, Dept. Mech. Eng., California Institute of Technology, Pasadena, CA, USA, 2006.

[26] X. Lin and S. Guo, "Development of a spherical underwater robot equipped with multiple vectored water-jet-based thrusters," *J. Intell. Robotic Syst.*, vol. 67, no. 3–4, pp. 307–321, Sep. 2012.

[27] D. S. Barrett, "Propulsive efficiency of a flexible hull underwater vehicle," Ph.D. dissertation, Dept. Ocean Eng., Massachusetts Institute of Technology, Cambridge, MA, USA, 1996.

[28] G. D. Weymouth, V. Subramaniam, and M. S. Triantafyllou, "Ultra-fast escape maneuver of an octopus-inspired robot," *Bioinspiration Biomimetics*, vol. 10, no. 1, p. 016016, 2015.

[29] F. Renda *et al.*, "Modelling cephalopod-inspired pulsed-jet locomotion for underwater soft robots," *Bioinspiration Biomimetics*, vol. 10, no. 5, p. 055005, 2015.

[30] F. Giorgio-Serchi, A. Arienti, and C. Laschi, "Underwater soft-bodied pulsed-jet thrusters: Actuator modeling and performance profiling," *Int. J. Robot. Res.*, vol. 35, no. 11, pp. 1308–1329, Sep. 2016.

[31] K. Mohseni, "Pulsatile vortex generators for low-speed maneuvering of small underwater vehicles," *Ocean Eng.*, vol. 33, no. 16, pp. 2209–2223, Nov. 2006.

[32] I. Vasilescu *et al.*, "Data collection, storage, and retrieval with an underwater sensor network," in *Proc. 3rd Int. Conf. Embedded Network. Sensor Syst.*, New York, NY, USA, 2005, pp. 154–165.

[33] A. Boch *et al.*, "A swarm of autonomous miniature underwater robot drifters for exploring submesoscale ocean dynamics," *Nature Commun.*, vol. 8, Jan. 2017, Art. no. 14189.

[34] T. Schmickl *et al.*, "CoCoRo the self-aware underwater swarm," in *Proc. 5th IEEE Conf. Self-Adaptive Self-Organizing Syst. Workshops*, Oct. 2011, pp. 120–126.

[35] T. Qiu *et al.*, "Swimming by reciprocal motion at low Reynolds number," *Nature Commun.*, vol. 5, Nov. 2014, Art. no. 5119.

[36] J. D. Moore and E. R. Trueman, "Swimming of the scallop, Chlamys opercularis (L.)," *J. Exp. Mar. Biol. Ecology*, vol. 6, no. 3, pp. 179–185, Apr. 1971.

[37] D. Donovan, J. P. Elias, and J. Baldwin, "Swimming behavior and morphometry of the file shell Limaria fragilis," *Mar. Freshwater Behav. Physiol.*, vol. 37, pp. 7–16, Mar. 2004.

[38] J.-Y. Cheng, I. G. Davison, and M. E. Demont, "Dynamics and energetics of scallop locomotion," *J. Exp. Biol.*, vol. 199, no. 9, pp. 1931–1946, Sep. 1996.

[39] D. M. Bailey and I. A. Johnston, "Scallop swimming kinematics and muscle performance: Modelling the effects of within-animal variation in temperature sensitivity," *Mar. Freshwater Behav. Physiol.*, vol. 38, no. 1, pp. 1–19, Mar. 2005.

[40] I. Tremblay, M. Samson-D, and H. E. Guderley, "When behavior and mechanics meet: Scallop swimming capacities and their hinge ligament," *J. Shellfish Res.*, vol. 34, no. 2, pp. 203–212, Aug. 2015.

[41] J.-Y. Cheng and M. E. DeMont, "Hydrodynamics of scallop locomotion: Unsteady fluid forces on clapping shells," *J. Fluid Mech.*, vol. 317, pp. 73–90, Jun. 1996.

[42] R. K. O'dor, "The forces acting on swimming squid," *J. Exp. Biol.*, vol. 137, no. 1, pp. 421–442, Jul. 1988.

[43] M. Sfakiotakis, A. Kazakidi, and D. P. Tsakiris, "Octopus-inspired multiarm robotic swimming," *Bioinspiration Biomimetics*, vol. 10, no. 3, p. 035005, 2015.

[44] A. A. Villanueva, K. J. Marut, T. Michael, and S. Priya, "Biomimetic autonomous robot inspired by the Cyanea capillata (Cyro)," *Bioinspiration Biomimetics*, vol. 8, no. 4, p. 046005, 2013.

[45] A. E. Carsen, B. G. Hatcher, and R. E. Scheibling, "Effect of flow velocity and body size on swimming trajectories of sea scallops, Placopecten magellanicus (Gmelin): A comparison of laboratory and field measurements," *J. Exp. Mar. Biol. Ecology*, vol. 203, no. 2, pp. 223–243, Oct. 1996.

[46] I. Tremblay and H. Guderley, "Scallops show that muscle metabolic capacities reflect locomotor style and morphology," *Physiological Biochem. Zoology*, vol. 87, pp. 231–244, Mar. 2014.

[47] Hydromea AUV technology. [Online]. Available: https://www.hydromea.com/

[48] C. W. Fay, R. J. Neves, and G. B. Pardue, "Species profiles: Life histories and environmental requirements of coastal fishes and invertebrates (mid-Atlantic): Bay scallop," U.S. Fish and Wildlife Service, Washington, DC, USA, Rep. FWS/OBS 82/11.12, 1983.